EPJ Web of Conferences **140**, 03042 (2017) DOI: 10.1051/epjconf/201714003042
Powders & Grains 2017

Shear localization and effective wall friction in a wall bounded granular flow

Riccardo Artoni[1,⋆] and *Patrick* Richard[1,⋆⋆]

[1] *LUNAM Université, IFSTTAR, MAST, GPEM, F-44340 Bouguenais, France*

Abstract. In this work, granular flow rheology is investigated by means of discrete numerical simulations of a torsional, cylindrical shear cell. Firstly, we focus on azimuthal velocity profiles and study the effect of (i) the confining pressure, (ii) the particle-wall friction coefficient, (iii) the rotating velocity of the bottom wall and (iv) the cell diameter. For small cell diameters, azimuthal velocity profiles are nearly auto-similar, i.e. they are almost linear with the radial coordinate. Different strain localization regimes are observed : shear can be localized at the bottom, at the top of the shear cell, or it can be even quite distributed. This behavior originates from the competition between dissipation at the sidewalls and dissipation in the bulk of the system. Then we study the effective friction at the cylindrical wall, and point out the strong link between wall friction, slip and fluctuations of forces and velocities. Even if the system is globally below the sliding threshold, force fluctuations trigger slip events, leading to a nonzero wall slip velocity and an effective wall friction coefficient different from the particle-wall one. A scaling law was found linking slip velocity, granular temperature in the main flow direction and effective friction. Our results suggest that fluctuations are an important ingredient for theories aiming to capture the interface rheology of granular materials.

1 Introduction

The rheology of granular materials is relevant to many industrials applications (grain transport and storage) and to natural events (avalanches, mud-slides…). Several geometries have been used to probe the rheology of granular systems (inclined plane, shear cell, confined gravity-driven flows…); however, a satisfying modeling of 3D flows is still lacking. This is particularly true for wall-bounded configurations, in which the nonlocality of the rheology near a boundary and the non trivial boundary conditions increase the complexity of the physics. In this work we present discrete element simulations of a wall-bounded three dimensional dense granular flow. The flow configuration studied in this paper, which can be referred as *torsional shear flow*, consists in a cylindrical geometry filled by the studied system, where the bottom wall rotates and the upper and cylindrical wall are fixed. In this work the flow is at fixed normal stress, i.e. the upper wall is free to move vertically under the action of the imposed normal force and the reaction of the particles contained in the cylinder. This configuration is interesting because simple velocity profiles were obtained for viscous and viscoelastic fluids, and therefore it is tempting to consider it as a granular rheometer. On the other hand, secondary flows were already observed for newtonian fluids in this geometry. The main objective of this work is therefore to characterize the granular flow in such a configuration. A particular focus will be given on the kinematics of the flow and on the flow regimes as a function of the main system parameters, and on the effective wall friction, and related scalings, at the cylindrical wall.

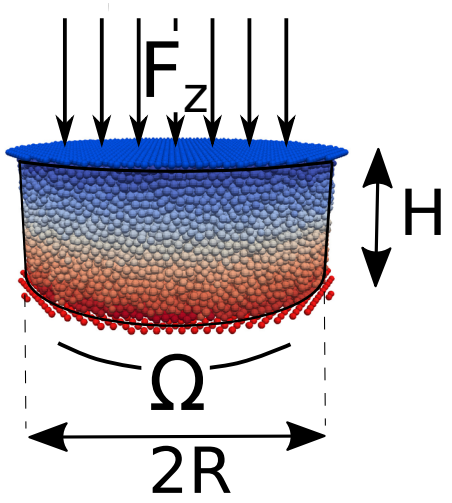

Figure 1. Sketch of the torsional flow configuration. F_z is the imposed normal force, and Ω the angular velocity of the bottom bumpy wall.

2 Simulation method

Numerical simulations are performed using the non smooth contact dynamics method [1], as implemented in the LMGC90 open source framework [2]. The flow configuration studied in this paper, which can be referred as

⋆e-mail: riccardo.artoni@ifsttar.fr
⋆⋆e-mail: patrick.richard@ifsttar.fr

© The Authors, published by EDP Sciences. This is an open access article distributed under the terms of the Creative Commons Attribution License 4.0 (http://creativecommons.org/licenses/by/4.0/).

torsional shear flow, consists in a cylindrical geometry where the bottom wall rotates and the upper and cylindrical wall are fixed. In this work the flow is at fixed normal stress, i.e. the upper wall is free to move vertically under the action of the imposed normal force and the reaction of the particles contained in the cylinder. The top and bottom walls are bumpy, while the cylindrical wall is smooth but frictional. Gravity acts on the system along z. The top wall cannot move on the x- and y- directions but is free to move in the z-direction, simply according to the balance between its weight, the externally applied force and the force exerted by the grains. Simulations were performed with N slightly polydisperse spheres (uniform number distribution in the range $0.9d - 1.1d$) interacting through perfectly inelastic collisions and Coulomb friction ($\mu_p = 0.5$). Each bumpy wall was composed of spheres with the same properties of the particles (positioned randomly with a surface density of approximately 0.2 spheres / d^2). We chose perfectly inelastic grains to maximize dissipation and thus save computation time. Interactions of particles with the flat walls were also perfectly inelastic and frictional (with a coefficient of friction μ_{pw}).

We performed several simulations varying the angular velocity of the bottom bumpy wall Ω, the force applied to the upper bumpy wall F_z, the particle wall friction coefficient μ_{pw}, and the radius of the cylinder R (while maintaining approximately the same system height $H \sim 20d$). The first two parameters can be made dimensionless for example by considering a particle Froude number $\tilde{\Omega} = \Omega R/\sqrt{gd}$ and the ratio between the total force mass exerted by the top wall and the weight of the grains, $\tilde{F} = \frac{Mg+F_z}{Nmg}$ where m is the average particle mass, and $M = 100m$ is the mass of the top wall. In particular, the investigated ranges correspond to $\mu_{pw} = 0 - 0.3$, $\tilde{\Omega} = 0.12 - 2.4$, $\tilde{F} = 0.2 - 100$, $R = 12 - 36d$ (corresponding to $N = 10000 - 90000$). Our simulations lie in a range of inertial number [3, 4] from 0 (for $r = 0$) to 10^{-1}, which corresponds to the quasistatic and dense regimes of flow. It is important to stress that, due to the cylindrical geometry, the inertial number is an increasing function of the radial coordinate.

3 Kinematic profiles

In the following, we report results on azimuthal velocity profiles. In order to compute such profiles, several snapshots of particle positions and velocities were extracted from the simulations at different times. Due to the axial symmetry of the flow geometry, averages were computed with respect to a grid in the (r,z)-plane; for each grid point the average velocity was computed by a space-time weighted average [5]. The time average was performed as a simple average of the space-weighted averages; for space averaging, on the other hand, a Heaviside step function around the grid point with diameter equal to one particle diameter was chosen. This corresponds to performing averages on toroidal volumes.

Autosimilarity of the profiles end effect of aspect ratio H/R. Figure 2 displays azimuthal velocity profiles

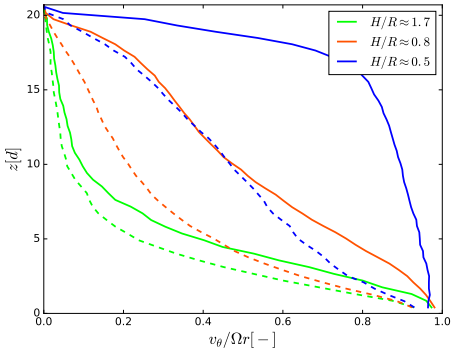

Figure 2. Azimuthal velocity profiles along z, rescaled by the velocity of the bottom wall, for $\tilde{\Omega} = 1.2$, $\tilde{F} = 0.2$, $\mu = 0.3$, three different values of the cell radius, and two radial positions, $1d$ from the cylindrical wall (dashed lines), and $10d$ far from the wall (solid lines).

rescaled by the velocity of the bottom plate, for $\tilde{\Omega} = 1.2$, $\tilde{F} = 0.2$, $\mu = 0.3$, three values of cell aspect ratio (at constant system height H). At first, the figure highlights the dependence of the velocity profile on the radial position: for large aspect ratios ($H/R = 1.7$), the velocity profile near the cylindrical wall is similar to the inner velocity profile. In this case, the velocity profiles are nearly autosimilar (see [6] for the dependance of the velocity with r). For smaller aspect ratios, the cylindrical wall slows down particle motion (in a well defined zone, not shown here, less than $10d$ thick, close to the wall), and this effect is stronger the smaller aspect ratio. Bulk profiles display a bottom localization for the large aspect ratio, a top localization for the small aspect ratio, and a more linear profile for the intermediate value. In the following, the effect of wall friction, pressure, bottom plate velocity will be evaluated for $H/R = 1.7$, and therefore, due to the near autosimilarity the profiles, rescaled azimuthal velocity profiles will be averaged in the radial direction.

Effect of wall friction coefficient and confining pressure. Figure 3 shows the joint effect of the particle-wall friction coefficient μ_{pw} and of the normal force applied to the top wall on the flow profiles, for $\tilde{\Omega} = 1.2$ and $H/R = 1.7$. For the sake of simplicity, due to the nearly autosimilarity of the profiles for this value of R, the profiles displayed in the Figure correspond to the average of the rescaled velocity profiles, $v_\theta/\Omega r$. First of all, profiles display shear localization with an exponential decay. However, the localization pattern depends strongly on wall friction. If we look at the behavior for low values of confining pressure (solid lines), for low wall friction, shear is localized near the top wall, while for strong friction shear is localized near the bottom wall. For intermediate values of the wall friction coefficient, a more uniform velocity profile prevails. As the wall friction coefficient, confinement pressure has a strong effect on velocity profiles: for negligible wall friction, increasing the normal force widens the top localized shear band. We can imagine that for very large confinement pressures and no wall friction the ve-

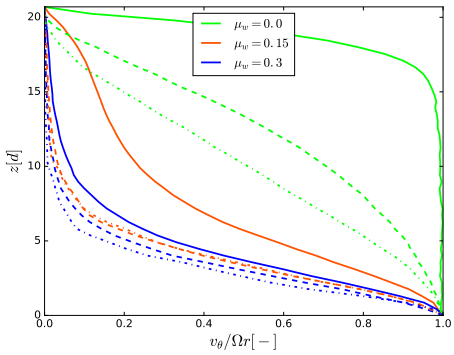

Figure 3. Average normalized azimuthal velocity profiles as a function of applied pressure, for $\tilde{\Omega} = 1.2$, $H/R = 1.7$, and three different values of the wall friction coefficient, and three different values of the force applied to the top wall : $\tilde{F} = 0.2$ (solid lines), $\tilde{F} = 8$ (dashed lines), $\tilde{F} = 100$ (dot-dashed lines).

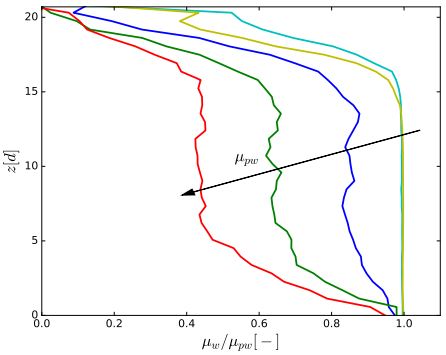

Figure 4. Profiles along z of the effective wall friction coefficient rescaled by the particle-wall friction coefficient μ_{pw} $(0.05, 0.1, 0.15, 0.2, 0.3)$, for $\tilde{\Omega} = 1.2$, $H/R = 1.7$, and different values of the wall friction coefficient μ_{pw}.

locity profiles will become linear. On the other hand, for larger values of the wall friction coefficient, increasing the normal force induces a strengthening of the bottom localization pattern with a decrease in the shear band width. The difference of the strain localization originates from the competition between dissipation at the sidewalls and dissipation in the bulk of the system [6, 14].

Effect of angular velocity and relevance of a local rheology. In the range of velocities considered here, the driving speed has little effect on the shape of velocity profiles (not shown). In [6], a model based on the $\mu(I)$ scaling and a minimum energy principle was developed. It was shown that, due to the presence of gravity, stresses are expected to increase with depth, and therefore the bulk energy dissipation is higher when shear is localized at the bottom. On the other hand, wall energy dissipation is higher if shear is localized near the top wall, because the plug flow zone contributes largely to the power needed to let particles slide at the wall, given that nearly all the particles at the wall slip with a large velocity. Changing the system parameters may change the relative balance of the two terms and therefore the shear localization pattern. The model was shown to predict the effect of pressure and wall friction, but wasn't able to capture the non-influence of the angular velocity of the bottom wall on the velocity profiles, at least without an ad-hoc correction.

This was explained by thinking at the combined effect of the rotating velocity and pressure. If the behavior of the system was described only by the characteristic inertial number and the wall friction coefficient, as a simple dimensional analysis could suggest, then we would expect that decreasing the rotational velocity by one order of magnitude should be the same as increasing the pressure by two orders of magnitude. But, as discussed above, the rotating velocity has no effect, while results are very sensitive to pressure, particularly for low wall friction. This means that the global inertial number and the wall friction coefficient are not sufficient for predicting the behavior of the system. It will be interesting to see if recent modelings of non-locality in granular flows [7–13] are able to capture the full behavior of our system.

4 Wall forces

We adapt here an analysis which we recently developed for a similar geometry [14]. We performed averages on slices with a thickness $2d$ in the vertical direction. The streamwise effective wall friction coefficient at the lateral walls is estimated for each slice as the ratio of the average force in the flow direction θ and the average force in the direction normal to the wall r: $\mu_w = \langle F_\theta \rangle / \langle F_r \rangle$ [15]. This corresponds to the stress ratio $\sigma_{r\theta}/\sigma_{rr}$ at the wall. Profiles of velocity fluctuations at the wall in the θ direction (which are related to granular temperature) are also calculated as $T_\theta = \langle (v_\theta - \langle v_\theta \rangle)^2 \rangle$, where $\langle v_\theta \rangle$ is the average azimuthal velocity of particle touching the wall for each slice. The fluctuations are correctly computed with respect to the average velocity value extrapolated at particle center [5].

Wall friction profiles. Figure 4 displays profiles of the effective wall friction coefficient, for $\tilde{\Omega} = 1.2$, $H/R = 1.7$, and different values of the wall friction coefficient μ_{pw}. It is clear that, as it was seen for 2D flows [16] or in 3D confined flows [14], μ_w/μ_{pw} decreases with μ_{pw}. These profiles are strongly related to velocity profiles: for low μ_{pw} (when shear is localized at the top), far from the shear band, grains rotate as a solid block with angular velocity Ω. In this case there are no stick events, so the effective coefficient of friction in the plug zone is equal to μ_{pw}. In the shear zone, stick-slip events may emerge, and therefore $\mu_w < \mu_{pw}$ [15]. For higher μ_{pw} values we find a decreasing profile of μ_w vs z in the shear band, a plateau in the center of the creep zone (intermediate z) and a decrease again when approaching the top wall. This can be explained by the fact that, reasonably, stick-slip events become more and more probable when we approach the creep zone [15].

Wall friction scaling. In [14], we found that μ_w/μ_{pw} scaled with a dimensionless parameter defined as the ratio between the slip velocty and the square root of the stream-

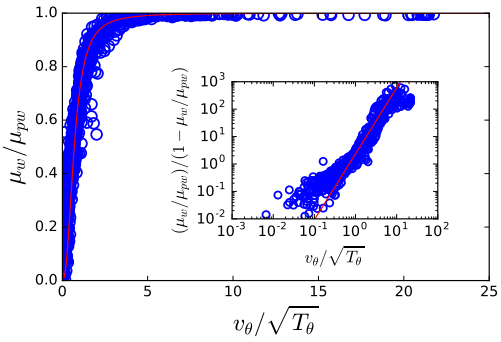

Figure 5. Rescaled effective wall friction coefficient versus the dimensionless slip parameter $v_\theta/\sqrt{T_\theta}$. The inset shows that a power law relationship holds between $\frac{\mu_w/\mu_{pw}}{1-\mu_w/\mu_{pw}}$ and $v_\theta/\sqrt{T_\theta}$. The solid line is a fit to Eq. 1, with $A = 0.7$ and $B = 2.4$.

wise velocity correlation. The origin of this scaling was postulated to be the presence of force and velocity fluctuations, yielding stick-slip events. Here we test the scaling for the present flow configuration. This test is shown in Fig. 5, where we display the rescaled effective friction coefficient μ_w/μ_{pw} as a function of $v_\theta/\sqrt{T_\theta}$. The scaling performs very well on several orders of magnitude. The functional form of the scaling appears to be the same as compared to the empirical one used in [14]:

$$\frac{\mu_w}{\mu_{pw}} = \frac{\left(v_\theta/\sqrt{T_\theta}\right)^B}{A + \left(v_\theta/\sqrt{T_\theta}\right)^B}, \qquad (1)$$

where $A = 0.7$ and $B = 2.4$ are best-fit parameters.

5 Conclusions

In this work, the rheological properties of granular matter submitted to torsional shear were investigated by means of discrete numerical simulations. The torsional shear flow configurations consists in a a shear cell made of a cylinder filled by grains which are sheared by a bumpy bottom and submitted to a vertical pressure which is applied at the top. An analysis of the kinematics of the system was presented. We focused on azimuthal velocity profiles and studied the effect of the confining pressure, the particle-wall friction coefficient, the rotating velocity of the bottom wall and the aspect ratio of the cell. For small cell diameters (large aspect ratio) profiles are nearly auto-similar, i.e. they are almost linear with the radial coordinate. Regimes differing by their strain localization features were observed : we find that shear can be localized (i) at the bottom or (ii) at the top of the shear cell, or that (iii) it can be even quite distributed. This interesting behavior originates from the competition between dissipation at the sidewalls and dissipation in the bulk of the system. A purely local rheology based on the inertial number I cannot predict the effect of the rotating velocity of the bottom wall: our results point out the need for an alternative rheology.

We also characterized the effective friction at the cylindrical wall. The strong link between effective wall friction, wall slip and fluctuations of forces and velocities was pointed out. At flat frictional walls, even if the system is globally below the sliding threshold, force fluctuations trigger slip events, leading to a nonzero slip velocity and an effective wall friction coefficient scaling with a sliding parameter. This confirms our previous findings in another flow configuration [14]: a scaling law was found linking slip velocity, granular temperature in the main flow direction and the effective friction. Our results suggest that velocity and force fluctuations can be an important ingredient for theories aiming to capture the interface rheology of granular materials.

Acknowledgements

The numerical simulations were carried out at the CCIPL (Centre de Calcul Intensif des Pays de la Loire) under the project MTEEGD.

References

[1] M. Jean, Computer Methods in Applied Mechanics and Engineering **177**, 235 (1999)
[2] M. Renouf, F. Dubois, P. Alart, Journal of Computational and Applied Mathematics **168**, 375 (2004)
[3] GDR-MiDi, Eur. Phys. J. E **14**, 341 (2004)
[4] F. da Cruz, S. Emam, M. Prochnow, J.N. Roux, F. Chevoir, Phys. Rev. E **72**, 021309 (2005)
[5] R. Artoni, P. Richard, Phys. Rev. E **91**, 032202 (2015)
[6] R. Artoni, P. Richard, Computational Particle Mechanics pp. 1–10 (2016)
[7] K. Kamrin, G. Koval, Phys. Rev. Lett. **108**, 178301 (2012)
[8] D.L. Henann, K. Kamrin, Proceedings of the National Academy of Sciences **110**, 6730 (2013)
[9] K. Kamrin, D.L. Henann, Soft Matter **11**, 179 (2015)
[10] D.L. Henann, K. Kamrin, Phys. Rev. Lett. **113**, 178001 (2014)
[11] J. Jenkins, D. Berzi, Granular Matter **12**, 151 (2010)
[12] J. Jenkins, D. Berzi, Granular Matter **14**, 79 (2012), 10.1007/s10035-011-0308-x
[13] R. Artoni, A. Santomaso, P. Canu, Phys. Rev. E **83**, 051304 (2011)
[14] R. Artoni, P. Richard, Phys. Rev. Lett. **115**, 158001 (2015)
[15] P. Richard, A. Valance, J.F. Métayer, P. Sanchez, J. Crassous, M. Louge, R. Delannay, Physical Review Letters **101**, 248002 (4) (2008)
[16] R. Artoni, A. Santomaso, M. Go', P. Canu, Phys. Rev. Lett. **108**, 238002 (2012)